Exploring Martian Magnetic Fields with a Helicopter

Anna Mittelholz, Lindsey Heagy, Catherine Johnson, Jonathan Bapst, Jared Espley, Abigail Fraeman, Benoit Langlais, Robert Lillis, William Rapin

The Planetary Science Journal, 4:155 (16pp), 2023 August https://doi.org/10.3847/PSJ/ace9c1

Exploring Martian Magnetic Fields with a Helicopter

Anna Mittelholz[1], Lindsey Heagy[2], Catherine L. Johnson[2,3], Jonathan Bapst[4], Jared Espley[5], Abigail A. Fraeman[4], Benoit Langlais[6], Robert Lillis[7], and William Rapin[8]
[1] Harvard University, Department of Earth and Planetary Sciences, Cambridge, MA 02138, USA; amittelholz@fas.harvard.edu
[2] Department of Earth, Ocean and Atmospheric Sciences, The University of British Columbia, Vancouver, BC, Canada
[3] Planetary Science Institute, Tucson, AZ, USA
[4] Jet Propulsion Laboratory, California Institute of Technology, Pasadena, CA, USA
[5] NASA Goddard Space Flight Center, Greenbelt, MD, USA
[6] Nantes Université, Univ. Angers, Le Mans Université, CNRS, LPG UMR F-6112, Nantes, France
[7] Space Sciences Laboratory, University of California, Berkeley, CA, USA
[8] IRAP, CNRS, Toulouse, France
Received 2023 May 3; revised 2023 July 11; accepted 2023 July 21; published 2023 August 29

Abstract

The era of helicopter-based surveys on Mars has already begun, creating opportunities for future aerial science investigations with a range of instruments. We argue that magnetometer-based studies can make use of aerial technology to answer some of the key questions regarding early Mars evolution. As such, we discuss mission concepts for a helicopter equipped with a magnetometer on Mars, measurements it would provide, and survey designs that could be implemented. For a range of scenarios, we build magnetization models and test how well structures can be resolved using a range of different inversion approaches. With this work, we provide modeling ground work and recommendations to plan the future of aerial Mars exploration.

Unified Astronomy Thesaurus concepts: Mars (1007); Solar system terrestrial planets (797); Planetary magnetospheres (997); Planetary science (1255); Planetary interior (1248); Planetary structure (1256)

1. Introduction

The recent successful deployment of the Mars helicopter Ingenuity (Balaram et al. 2021) and the decision to augment and back up planning for Mars sample return with fetch helicopters has opened new possibilities for future science-driven aerial exploration of Mars. Magnetometers are ideal science instruments that can exploit new helicopter technologies and provide data that could address a range of key questions regarding ancient and present Mars (Bapst et al. 2021; Mittelholz et al. 2021a; Rapin et al. 2021; Mitteholz & Johnson 2022). Crust, once magnetized by an internally powered dynamo, holds information about the interior and surface conditions at the time magnetic layers were emplaced and the processes, e.g., volcanic or impact, that have modified the crust since (Mitteholz & Johnson 2022). Environmental conditions, such as surface chemistry or the availability of water, influence processes that could have led to the acquisition and/or modification of crustal magnetization. Global magnetic fields are linked to atmospheric processes because of the degree to which atmospheric escape channels are enhanced or suppressed in the presence or absence of a dynamo field (Brain et al. 2013; Brain et al. 2016; Ramstad & Barabash 2021). From the perspective of upcoming human exploration, characterization of small-scale crustal magnetization is essential to (i) identify iron-bearing materials for potential resource exploration and (ii) explore the effects of magnetic shielding from harmful solar and cosmic energetic charged particles. Magnetic fields are thus a fundamental component of planetary systems, and investigating them contributes to the understanding of planetary evolution and current state.

Globally, the most comprehensive Martian magnetic field information comes from fluxgate magnetometers on orbiters, specifically the Mars Global Surveyor (Acuña et al. 1999) and Mars Atmosphere and Volatile Evolution (Jakosky et al. 2015) missions, as well as the recent Chinese Tianwen-1 orbiter (Liu et al. 2020). Locally, the lander Interior evolution using Seismic investigation, geodesy and heat transfer (InSight; Banerdt et al. 2020) measured the magnetic field at the landing site in Elysium Planitia, providing the first surface magnetometer data from Mars (Johnson et al. 2020). More recently, the Chinese Zhurong rover has added several data points of the horizontal magnetic field components along its traverse in the Utopia basin (Du et al. 2023). Lastly, meteorites have contributed to our understanding of magnetic carriers and paleofields, and despite large uncertainties in provenance, they provide the only samples that can be analyzed in laboratories (Cisowski 1986; Kirschvink et al. 1997; Shaw et al. 2001; Antretter et al. 2003; Gattacceca et al. 2013; Volk et al. 2021).

Crustal magnetic field investigations address fundamental questions of interest to the planetary and particularly Mars community as defined by the Mars Exploration Program Analysis Group (MEPAG; Yingst et al. 2022) as shown in Table 1: (1) the formation and evolution of the crust, including its mineralogy and modification over the past 4.5 Gyr, by tectonic, impact, fluvial, hydrothermal, and magmatic processes (MEPAG Goal III, Objectives A+B); (2) the evolution of the core dynamo and its implications for core composition and dynamics; interior evolution including early global heat flow, mantle dynamics, and tectonic regime (e.g., whether Mars had an early phase of plate tectonics; MEPAG Goal III, Objective B); (3) the link between atmosphere evolution and the extinction of the Martian dynamo and thus important information on habitability (MEPAG Goal II, Objective C); and (4) implications for future human exploration (MEPAG Goal IV, Objective A).

Table 1
Scientific Traceability of Magnetic Field Measurements; Scientific Questions Are Related to (M) Magnetization, (D) Dynamo and (HE) Human Exploration

MEPAG Goal and Objective	Scientific Questions	Observable Quantities	Possible Issues	Additional Instrumentation and Mitigation Strategies
MEPAG Goal III: understand the origin and evolution of Mars as a geological system	Crustal composition: (M1) What are the carriers of magnetization?	• Magnetized surface feature • General geochemical analysis of the mineralogy of the crust (no matter if magnetized)	Surficial mineralogy not necessarily representative; buried layers cannot be accessed	Spectrometers for analysis of elemental and mineralogical composition
Objective A: document the geologic record preserved in the crust and investigate the processes that have created and modified that record	(M2) Magnetization strength: what gives rise to strong magnetization? Is it a thick magnetized layer, distinct mineralogy, or a combination thereof?	• Magnetized feature of known volume such as pebble/clast. • Magnetized layer for which depth/volume can be approximated, e.g., magnetic field observations at varying survey altitudes.	Pebble/clast not magnetized; volume of features not easy to evaluate	• Imagery to identify pebbles/clasts or layering and approximate volume. • Gravimeter to approximate density/composition of magnetized feature. Joint inversion can potentially aid in 3D modeling of underlying magnetized volume. • Spectrometers to get insight on composition/magnetization carrier.
	Crustal creation and modification: (M3) What are the dominant magnetization acquisition mechanisms? How do they vary?	Measure magnetic field in different geological settings, e.g., volcanic versus aqueous alteration	Source of magnetization not easily identifiable, e.g., magnetization originates at depth (i.e., hydrothermal versus volcanic intrusion)	• Mineralogy and imagery to identify origin of material, i.e, surficial volcanic versus altered rock. • Gravimeters can provide information on subsurface density and thus carry information on rock type and alteration state.
	(M4) What are the typical length scales of magnetization?	Magnetic field changes along the flight path if possible at different altitudes and in comparison with previous landed/orbital measurements	Possible lack of changes along path; especially if in-flight not an option, ROI measurements too limited?	Multiple orthogonal flights over a given region
Objective B: determine the structure, composition, and dynamics of the interior and how it has evolved	Global planetary evolution: (D1) When did the dynamo operate?	• Magnetized dateable feature at surface. • Clear demagnetization signature indicating that surface layer is magnetized. • Age constraints on magnetized and unmagnetized units.	No surface magnetization	Gravimeter: identify the magnetized source body by identifying units of different density and thus potential to infer composition

Table 1
(Continued)

MEPAG Goal and Objective	Scientific Questions	Observable Quantities	Possible Issues	Additional Instrumentation and Mitigation Strategies
	(D2) Dynamo characteristics: did the polarity change? How strong was the dynamo field? What are the driving mechanisms?	• Identify magnetized dateable layers. • Evaluate magnetization for observable volume to infer dynamo strength.	No observable layering; no surface magnetization	Imagery to identify dateable surface features to be linked to the presence or absence of magnetization associated with the feature
MEPAG Goal IV: prepare for human exploration Objective A: obtain knowledge of Mars sufficient to design and implement human landing at the designated human landing site with acceptable cost, risk, and performance.	(HE1) How deep in the crust are iron-bearing mineral resources? (HE2) What is the radiation environment on the Martian surface?	Low-altitude vector magnetic field survey	If in-flight not an option, ROI measurements too limited?	• Gravimeter: identify the magnetized source body by identifying units of different density and enable joint inversions. • Measurements at multiple altitudes to better constrain the source region.

Here we summarize key questions in Mars magnetism linked to broader questions about planetary systems as defined by MEPAG and point out key observables that would allow these questions to be addressed using low-altitude measurement platforms (Table 1). We refer to Mitteholz & Johnson (2022) for a more detailed discussion of magnetic data sets, what we have learned from them, and remaining key knowledge gaps. The dynamo (D1 and D2 in Table 1) provides important information on early Mars evolution for which the dynamo timing, driving mechanisms, and possible changes in polarity and strength are key constraints. MEPAG Goal III.B clearly motivates investigation of the evolution of the ancient Martian dynamo and the manner and timing of its demise. Clues to this lie in the crustal material that was magnetized by the dynamo magnetic field (M1–M4 in Table 1). Further, although we know that the Martian crust is strongly magnetized in some places, we do not know the origin of this magnetization. There is a general understanding of possible magnetic carriers from meteorites and consideration of the Martian redox state (Dunlop & Arkani-Hamed 2005; Rochette et al. 2005; Tikoo & Evans 2022), but we do not know the source mineralogy of the anomalies (M1 and M2) or the process(es) that magnetized the rocks (M3). MEPAG Goal III.A points out the importance of investigating the geological record preserved in the crust and magnetization as an important characteristic that contains information on the time the crust formed, as well as how it was modified over time and in response to heat, water, and/or shock. Further, the connection to ancient climate as highlighted in MEPAG Goal II.C is twofold. First, the shutdown of the dynamo and loss of the global magnetic field would have fundamentally altered the rate and manner of atmospheric escape (Ramstad & Barabash 2021), but although a connection has been hypothesized, the degree of connection between the dynamo and the Martian climate is unclear. However, to address this question, timing constraints as discussed in D1 are essential. Second, magnetization acquisition processes involving water as discussed in M3 would (if important) be interconnected with an ancient hydrosphere. This MEPAG goal is not explicitly listed in Table 1 due to its interconnections with previous questions. Lastly, in preparation for future human exploration (MEPAG Goal IV), geophysical characterization of the subsurface and possible identification of iron-bearing material resources are of importance for future human settlement efforts (HE1). So is a good understanding of local-scale (kilometers to tens of kilometers) crustal magnetic fields, which might provide protection from radiation (HE2). The degree of this protection has been shown to strongly depend on crustal field geometry (Emoto et al. 2018). With a lack of understanding of the strength, distribution, and geometry of surface magnetic fields, this question cannot be sufficiently addressed.

Existing magnetic field data sets, as well as magnetic field and magnetization models developed from them, provide context for regional studies that can capture information at spatial scales >100 km. However, investigating smaller-scale magnetic fields on Mars can provide information that simply cannot be gleaned from orbit. A well-known terrestrial analog is the pattern of alternating linear marine magnetic anomalies with a horizontal extent of ~20 km ("magnetic stripes") parallel to mid-oceanic ridges that provided key supporting evidence for both plate tectonics (Vine & Matthews 1963) and global magnetic field reversals. These signals are revealed in shipboard and aircraft survey data but are not detectable from satellite orbit altitudes (Ravat 2011).

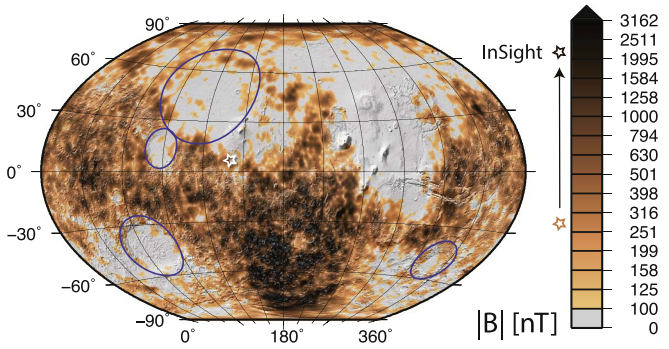

Figure 1. Magnetic field amplitude, |B|, from a satellite data-based model, downward continued to the surface (Langlais et al. 2019). The star represents the InSight landing site, with the model surface prediction of ~300 nT vs. the actual ~2000 nT measured by InSight's magnetometer. The circles outline the big impact basins Hellas, Utopia, Argyre, and Isidis for context.

Although existing magnetic field data have provided invaluable information on the Martian crustal magnetic field (and more), each data set has distinct and serious limitations. Satellite data provide a global picture but can only resolve scale lengths comparable to orbital altitudes; for Mars, this is typically 100–200 km. Lander measurements such as those provided by InSight give only a single-point measurement of the crustal magnetic field. A single-location measurement may be explained by a large number of magnetization models, requiring further constraints on the volume and location of the magnetized source rock, to constrain the possible parameter space (Johnson et al. 2020; Knapmeyer-Endrun et al. 2021; Wieczorek et al. 2022). Rover observations, such as the data from Zhurong, cover limited distances (hundreds of meters to tens of kilometers), are surface observations (no vertical distribution of measurements), and can only be obtained in terrain that is accessible to rovers, i.e., less than ~25° slopes. A helicopter is the ideal platform to overcome such limitations; it enables comprehensive aerial surveys at low altitudes that can detect unexplored signals, bridging the gap between surface and orbital observations. In addition, it can traverse any terrain, including the steep walls of valleys, canyons, and craters, in addition to dune and boulder fields and other hazardous terrain.

As a first step toward realizing a magnetic helicopter mission, we need to consider the types of data sets and modeling techniques that we might be able to exploit. Magnetic field modeling on Mars has mostly been based on orbital vector magnetic field data so far, and different modeling approaches have been used to build local and global models of the magnetic field (e.g., Figure 1). One common class of models are parameterized by spherical harmonics that are fit to the data and produce a model of the magnetic field (e.g., Cain 2003; Morschhauser et al. 2014). Others have used equivalent source dipole models (Mayhew 1979) for which the magnetic moments of dipoles in a single subsurface layer are fit to the satellite observations (e.g., Purucker et al. 2000; Mittelholz et al. 2018; Langlais et al. 2019). While these models solve for possible magnetization distributions from which the magnetic field can be predicted, they suffer from nonuniqueness; i.e., a very wide range of crustal magnetization distributions can result in the same pattern of fields measured from orbit. In other words, these models cannot resolve 3D structure given their large receiver–source distances.

Further, different models use different inversion approaches. For example, the use of different norms largely influences how localized anomalies appear in a given model. The most classic models use least-squares or L2 norms and create smooth models (e.g., Mittelholz et al. 2018; Langlais et al. 2019). An iterative approach of different model norms was applied by Morschhauser et al. (2014) aiming for a better representation of localized anomalies compared to L2 models. Others have created sparse models using an L1 norm, and such models favor compact anomalies (Moore & Bloxham 2017). While these approaches provide different magnetic field models, they all are consistent with the data. Hence, the choice of model norm guides the nature of the recovered model.

Potential field data do not intrinsically have depth resolution, and the nonuniqueness of different models is an inherent property of such fields. However, data collected at lower and variable altitudes and with denser coverage would enable high spatial resolution; thus, more targeted questions could be addressed. Methods for inverting such data sets to obtain 3D models are advanced in terrestrial geophysics, which will aid us in the interpretation of such models. Thus, a helicopter magnetic field data set will allow the characterization of crustal magnetization in unprecedented detail and the construction of significantly higher-resolution models, both horizontally and vertically. That is, there is no substitute for low-altitude in situ measurements of crustal magnetic fields.

In this paper, we discuss example crustal magnetization scenarios and survey designs for future aerial surveys with a focus on helicopters. Many aspects explored in this paper are applicable to other low-altitude platforms, such as balloons (Hall et al. 2007) or airplanes (Braun et al. 2006). We first discuss the magnetic field we might expect to measure using a helicopter-borne magnetometer and include magnetic field contributions from crustal magnetization and magnetic noise. We explore three geological scenarios and different survey geometries and investigate how well magnetized structures can be recovered in models. In the light of helicopter data sets that might comprise sparse data compared to terrestrial regional surveys, we examine a range of inversion methodologies and discuss ways in which different inversion approaches can identify different types of structures for our hypothetical scenarios. Finally, based on our modeling efforts, we offer recommendations for a future helicopter mission to Mars.

2. A Helicopter Mission on Mars

2.1. Helicopter Mission Concepts

Future Mars helicopter missions include Sample Recovery Helicopter–like vehicles (Mier-Hicks et al. 2023), capable of carrying up to 1 kg of payload tens to hundreds of kilometers for a standard mission duration (∼1 Mars year), or larger Mars Science Helicopter concepts that are capable of carrying up to 5 kg of payload hundreds of kilometers (Bapst et al. 2021). Both would enable low-altitude coverage (up to several hundred meters) and offer the possibility of surveying the magnetic field of Martian regions in an unprecedented manner. Because magnetometers are lightweight and consume little power, and they can take advantage of low-altitude aerial mapping, we will now focus on discussing these highly relevant mission strategies.

A possible survey strategy includes several regions of interest (ROIs) that can be defined in advance using results from orbital data depending on the overall mission goals. The helicopter can perform in-depth analysis of those ROIs using its full instrument suite in conjunction with local/regional context from flight traverses (Figure 2(a)).

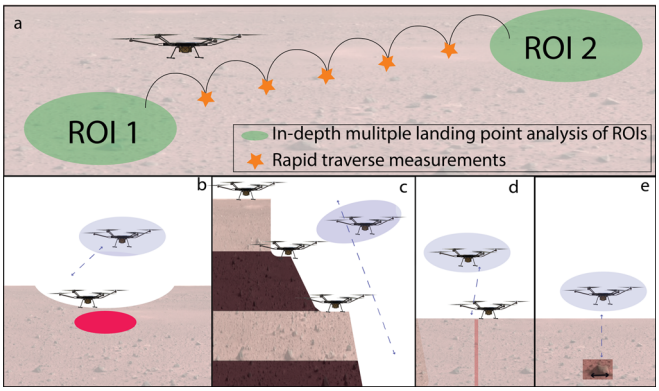

Figure 2. Helicopter scenarios. Blue shading represents measurements taken in flight. (a) Representation of different sampling scenarios between ROIs. Panels (b)–(d) are the scenarios modeled in Section 3 and represent a magnetized crater, differently magnetized layers, and a magnetized dike intrusion; panel (e) represents surveying of individual pebbles.

Here we explore three magnetic field data set scenarios. In the first, we construct gridded data sets that provide evenly distributed measurements. The data sets and resulting inversions can be compared with those from more realistic survey strategies: one for which data are only collected on the ground and when the helicopter is not moving and one in which in-flight measurements are also possible. The latter option requires a more advanced magnetic cleanliness program (discussed in Section 5) but can take full advantage of the complete flight path.

2.2. Magnetic Field Contributions

Generally, contributions to the overall measured magnetic field are of spacecraft and Mars external and internal origin, i.e., sources above and below the planetary surface, respectively. We assume that helicopter-generated fields can be characterized and subtracted, and only naturally occurring fields are discussed. For a typical helicopter survey, mapping of the crustal magnetic field would be the primary mission objective, but regardless of whether external fields are of interest by themselves, separating internal and external contributions is required.

The internal magnetic field depends on the location of the measurement and, due to the absence of a Martian dynamo field, results solely from crustal magnetization. Amplitudes of the crustal magnetic field vary greatly, and satellite data-based surface predictions range from zero to 12,000 nT with an average and median of 450 and 200 nT, respectively (Figure 1; Langlais et al. 2019). However, those predictions are based on orbital data that are insensitive to small-scale (<∼100 km) magnetization. At the InSight landing site, the predicted magnetic field amplitude (Smrekar et al. 2018) was approximately 10% of the observed ∼2000 nT (Johnson et al. 2020). The strength of the predicted field at InSight is close to the global median value, and we might thus expect to find many similar and even stronger fields at the Martian surface. However, in less magnetized regions, such as in the northern hemisphere, crustal fields at the surface could be close to zero.

Table 2
Time-varying Magnetic Field Contributions Measured on the Surface by InSight

Phenomenon	Magnetic Signal	Notes
Daily: ionospheric currents	Typical peak amplitudes up to 40 nT	Magnetic fields driven by ionospheric currents are minimal during the nighttime and peak in the early to mid-morning
Short-period waves or pulsations: magnetic fields driven by interaction of magnetosphere with solar wind	Typical peak amplitudes up to a few nT with periods of hundreds to thousands of seconds	Typically observed at dust/dawn and around midnight on horizontal components
Transient sources: solar events	Increased peak diurnal amplitudes in all components; nighttime fluctuations (periods ∼20–30 minutes) up to ∼10 nT	Solar events can be predicted and tracked but have an effect for multiple days
Transient sources: dust movement	Small-amplitude signals <0.5 nT for ∼10 seconds	The frequency of such events would likely depend on dust availability at the landing site.

This is, for example, the case for the Zhurong measurement sites (Du et al. 2023).

External magnetic fields at the surface can be of periodic nature, e.g., due to ionospheric currents (Lillis et al. 2019; Johnson et al. 2020; Mittelholz et al. 2020b), the interplanetary magnetic field (Langlais et al. 2017; Luo et al. 2022; Mittelholz et al. 2023), or transients, such as space weather (Mittelholz et al. 2021b) or dust movement (Thorne et al. 2022). InSight provides surface observations over a prolonged time frame, and although external field phenomena are summarized elsewhere (Mittelholz et al. 2023), we list them in Table 2 to assess how large their contributions might be and whether they would affect crustal magnetic field measurements. Note that a different crustal magnetic field environment (that is, in a different location) would affect ionospheric currents and the resulting magnetic fields (Lillis et al. 2019).

Short-period fluctuations are observed at dusk/dawn and around midnight. Even if measurements were taken during those times, the fluctuations are on the order of only a few nanoteslas (Chi et al. 2019; Johnson et al. 2020). Daily fluctuations due to ionospheric currents, however, could lead to signals of tens to hundreds of nanoteslas depending on the strength of the background magnetic field and season (Lillis et al. 2019; Mittelholz et al. 2023). For InSight, daily fluctuations have been found to vary with season and dust content, and individual days can vary by tens of nanoteslas (Mittelholz et al. 2020b). Longer-period fluctuations associated with the interplanetary magnetic field are small at the InSight landing site, and their effect is likely negligible (Mittelholz et al. 2023). For a helicopter survey, identification and characterization of transient sources are unlikely to present a challenge because their amplitude is either too small, e.g., dust devils (Thorne et al. 2022), or, for ionospheric and magnetospheric currents, they can be either recognized by their time/diurnal profile or avoided/ignored during times of space weather (Mittelholz et al. 2021b).

The effect due to spatially and temporally varying magnetic field fluctuations depends on whether data are collected in flight or while landed at ROIs only. For landed measurements, i.e., measurements taken when the helicopter or rotor system is not moving, contributions to the measured magnetic field consist of the crustal magnetic field at that specific landing site and time-varying magnetic fields over a longer time frame (Table 2). Especially if the helicopter collects data during the nighttime, the time-varying external field contributions are minimal and can easily be identified and subtracted from the crustal contribution. For in-flight measurements, subtracting external fields would be more challenging, as the internal field also varies as the helicopter flies across varying crustal magnetic anomalies. Generally, to separate internal and external fields we recommend repeat measurements covering ROIs several times and at magnetically quiet periods, and vertical flights at several locations across the region.

Finally, crustal contributions are expected to outweigh external field contributions at many locations. Landed measurements enable individual robust crustal field measurements because time-varying magnetic fields can be readily identified, especially during magnetically quiet nights. Tracking of diurnal fluctuations while on the ground could then inform on spatially varying crustal fields versus external variations for in-flight measurements. Additional data collected during the traverse would ensure dense coverage of flight paths between landed measurements and enable crustal magnetic field characterization of unprecedented resolution.

2.3. Helicopter Magnetic Field Surveys

One advantage of airborne surveys is the traversability in any terrain, such as boulder fields and along steep walls. We present a range of geological settings that one could encounter on Mars and for which magnetic signatures might be expected. First, magnetization associated with craters (or the lack of magnetization) has been used previously to constrain the timing of the dynamo (Lillis et al. 2013; Vervelidou et al. 2017; Mittelholz et al. 2020a). This addresses questions D1 and D2 in Table 1. (De)magnetization signatures associated with crater interiors arise due to the effect of shock and heating during an impact (Mohit & Arkani-Hamed 2004; Gattacceca et al. 2008). Excavation of magnetized material can also have an effect (Mittelholz et al. 2020a; Ojha & Mittelholz 2023), and this has been used to constrain the dynamo to 3.7 Ga. Craters on Mars are ubiquitous (Robbins et al. 2013), and any landing site would likely offer the opportunity to traverse impact craters and ejecta. As such, in this scenario, we can test if a dynamo operated at the time of the impact. A test of magnetizations of features (not necessarily craters) of several different ages is necessary to construct a timeline of the Martian dynamo and help constrain the evolution of the interior state of Mars, i.e., changing from sustaining a dynamo to being unable to do so. Hence, this is a highly relevant scenario for any future mission with a magnetic focus.

In a second scenario, we investigate the magnetization signature of a dike intrusion. Generally, magmatic activity throughout Martian history is evident (Tanaka et al. 2014), and dikes have been mapped in volcanically active areas such as Tharsis (Brustel et al. 2017; Pieterek et al. 2022) or indirectly inferred from rift structures or seismic data (Nimmo & Stevenson 2000; Stähler et al. 2022). Magnetization associated with dateable volcanic features can address volcanic and dynamo evolution (Johnson & Phillips 2005; Lillis et al. 2006; Mittelholz et al. 2020a). Again, this is linked to questions D1 and D2, but especially in comparison with the above examples, it allows one to characterize magnetization that is known to be linked to thermal effects as opposed to a site in which one observed clear signs of shock or alteration (questions M1–M4). For example, the analysis of the magnetic field of a dike could reveal a demagnetization signature for a young intrusion in a magnetized layer or a magnetization signature if the intrusion and the surrounding layer were emplaced while a dynamo was active. Furthermore, ferrous mineralogies of the dike could enhance the magnetization compared to the background. Moreover, this particular example is defined to address resolvability, i.e., how well very small features can be resolved, irrespective of the science question asked.

Lastly, we consider layering that could be found in a valley or graben structure (Nedell et al. 1987; Le Deit et al. 2010). This would offer ideal conditions to traverse multiple layers of different ages to establish a magnetic timeline and address the question of dynamo activity and possible polarity changes over the range of emplacement ages represented in the set of strata (D2). At least one polarity change has been hypothesized based on orbital data and the meteorite ALH84001 (Thomas et al. 2018; Steele et al. 2023); testing the characteristics of a dynamo over time would provide unprecedented information on interior evolution. Stacked layers of different material and possibly different origins would further allow one to address all questions labeled M in Table 1. From a more technical perspective, this scenario also allows intuition to be gained on expected magnetic signals across at least two distinct blocks of magnetization.

3. Modeling Approach

3.1. Background

In preparation for future missions, in this study, we model the proposed scenarios and perform inversions to investigate the degree to which we can recover magnetized structure. We use the open-source SimPEG package in Python (Cockett et al. 2015), and an example code is available online. First, we simulate magnetic field data collected by a helicopter above a given magnetization model; this is the forward problem. From Gauss's law, the relation between magnetization per unit volume M in Am^{-1} and magnetic field B in teslas is

$$\boldsymbol{B}(r) = \frac{\mu_0}{4\pi}\int_V \nabla\nabla\frac{1}{r}\cdot\boldsymbol{M}dV, \tag{1}$$

where r is the radial distance between the measurement point and the magnetic source of volume V, and μ_0 is the magnetic permeability of free space. Using simulated data, $\boldsymbol{d}$, we then aim to recover our model, $\boldsymbol{m}$, by solving an inverse problem. First, we define the parameters we aim to estimate by solving the inverse problem. We use a voxel model of the subsurface, where each cell has a vector magnetization that we seek to estimate (Lelièvre & Oldenburg 2009). The inverse problem is nonunique and underdetermined; i.e., there are infinite possible solutions. Therefore, one needs to incorporate additional constraints. Traditionally, the inverse problem can be formulated as an optimization problem (Tikhonov et al. 1995) in which one can impose regularization and minimize an objective function that contains a data misfit term, Φ_d, and a model regularization term, Φ_m. The trade-off parameter β controls the relative importance between the two competing terms, and Φ_d^* represents an acceptable target misfit:

$$\min\Phi(m) = \Phi_d + \beta\Phi_m \quad \text{subject to} \quad \Phi_d \leqslant \Phi_d^*. \tag{2}$$

The first term, Φ_d, describes the misfit between observed, d_{obs}, and predicted, d_{pred}, data,

$$\Phi_d = \sum_{i=1}^{N}\frac{(d_i^{\mathrm{pred}} - d_i^{\mathrm{obs}})}{\sigma_i}, \tag{3}$$

normalized by estimated uncertainties σ for each data point i. Assuming that the noise and error on the data are random, the expected target misfit $\Phi_d^* = N$, where N is the number of data.

The second term penalizes differences between the model and a reference model and can be made up of several functions that control the magnitude and roughness of the model,

$$\Phi_m = \sum_{r=s,x,y,z}\int_V w_r|f_r(m)|^{p_r}dV, \tag{4}$$

where f_r consists of one or more of $f_s = m$, $f_x = dm/dx$, $f_y = dm/dy$, and $f_z = dm/dz$, describing the smallness and roughness in all orthogonal directions. The weighting term w_r adjusts the importance of the regularization terms. Lastly, we use the general l_p norm, which can be independently adapted for the different regularization functions with $0 \leqslant p_r \leqslant 2$.

In order to minimize Equation (2), we discretize our model onto a tensor mesh and find a solution such that the gradient of the objective function $\nabla_m\Phi(\boldsymbol{m}) = 0$. The trade-off parameter β is decreased until a defined threshold tolerance is reached or after a given maximum number of iterations. The inexact Gauss–Newton algorithm is used to calculate appropriate model updates; for more details on the inversion, we refer the reader to Fournier & Oldenburg (2019).

3.2. Survey Geometry and Model Setup

We simulate three different survey geometries with a decreasing number of measurements for each of the scenarios described in Section 2.1. First, we construct a regular tensor mesh across the ROI and simulate the data that would result from the magnetization model if the data were collected on an idealized grid (Figures 4(a) and (b)). For example, for the crater scenario, the survey includes 15 × 15 data points across a 600 × 600 m area, resulting in 225 data points (Figures 4(b) and (f)). The next survey geometry simulates the flight path of a helicopter; the helicopter lifts off the ground up to an altitude of 10 m at the center point of each track before it lands. We simulate three tracks with 30 data points on each (Figures 4(c) and (g)). Note that changing altitude contributes to the magnetic field observation; i.e., the magnetic field signal is decreased at times when the helicopter is further away from the surface and the source of magnetization. With an approximate helicopter speed of 10 $\mathrm{m\,s}^{-1}$, the 30 data points across 10 m equate to a sampling rate of 30 samples s^{-1}. Lastly, we explore

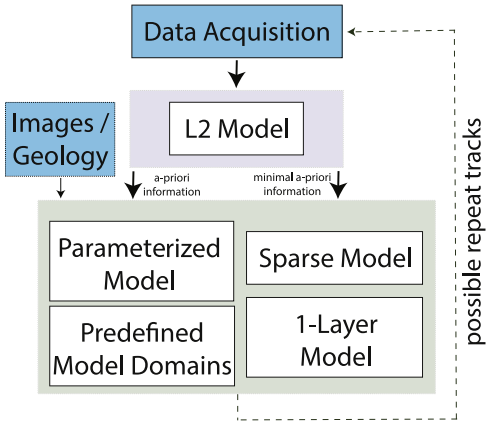

Figure 3. Inversion strategy.

the scenario in which the helicopter only collects data on the ground (i.e., when it is not flying). Six measurements at discrete locations are collected in this survey (Figures 4(d) and (h)). For all models, we assume background noise with a standard deviation of 0.1 nT, but we vary this parameter in Section 5.1.

3.3. Modeling Strategy

We propose a modeling strategy in which different inversion techniques are applied consecutively to achieve confidence in the recovered magnetization and inferred geological models (Figure 3). While some techniques rely on no or minimal a priori information, we also show examples of how a priori information, i.e., information from other data sets, particularly imagery, can be incorporated into the inversion. As sketched in Figure 3, after data acquisition, we initially generate a smooth L2 inversion for a first estimate of the distribution of magnetization and its possible relation to observable surface structures (Section 3.3.1). Next, we aim for a model that will highlight contrasts and produce compact structure in a sparse inversion (Section 3.3.2). We then incorporate knowledge of geological structure or layering in the inversion (Sections 3.3.3, 3.3.4, and 3.3.5). Different techniques are briefly described below and later applied to the different scenarios to showcase the range of different inversion strategies.

3.3.1. Smooth Inversions

Traditionally, an L2 norm is used for the regularization term (Equation (4)); i.e., p_r is set to 2. The L2 inversion results provide a smooth picture of the magnetization, which, in the case of structure that extends at depth or does not have clearly defined edges, can provide an adequate model. With no prior information, we consider this a good first approximation and perform such an inversion for each scenario. However, L2 modeling can smear out compact features and be too smooth to be geologically interpretable.

3.3.2. Sparse-norm Inversions

We also explore more compact solutions with $0 \leqslant p_r < 2$. For small p_s, the inversion favors compact anomalies with large physical property contrasts, while reducing the $p_{x,y,z}$ values generates flat anomalies with sharp edges along the Cartesian directions. These approaches do not require prior information. However, in both types of inversion, regularization can be tuned to, for example, emphasize compactness in particular directions because different regularization terms have their individual weighting terms. More details on this inversion and a comparison to the smooth L2 inversion as implemented in SimPEG are provided in Fournier et al. (2020).

3.3.3. Single Layer

Crustal magnetic field models on Mars have so far used a single layer of dipoles, not attempting to resolve 3D structure with low-resolution satellite data, thus providing an integrated picture of the subsurface (e.g., Vervelidou et al. 2017; Mittelholz et al. 2018; Langlais et al. 2019). This simplified approach can be a useful tool in identifying the horizontal extent of magnetization in the subsurface without attempting to resolve 3D structure, i.e., thickness and lateral variations of magnetization at depth. Because this strategy greatly reduces the model space, it can be useful to quickly gain insight into any relationships between surface geology and magnetization. We adapt this strategy for the intrusion scenario and implement a 1 voxel vertical layer of elongated cuboids. While one can perform smooth or sparse model inversions, we only show results for the smooth solution.

3.3.4. Parametric Model

For a simple and well-constrained geological structure, additional information may allow parameterization of the model with only a few variables while keeping the surrounding structure parameterized with voxels. This greatly reduces the number of model parameters and can convert the underdetermined problem into an overdetermined problem, for which regularization is not necessary. Images outlining, e.g., a dike or crater, i.e., prior information on the magnetization geometry, are applications in which this approach can be useful. In our example, we will represent the crater by a half-sphere and can describe it by its center location in 3D [x, y, z]; its radius, r; and its magnetization vector [m_x, m_y, m_z]. Note that this approach may be combined with, e.g., a smooth inversion and used as a hybrid approach when only part of the subsurface is well constrained (Herring et al. 2022).

3.3.5. Domain Mapping

Lastly, if distinct units are observed that might be uniformly magnetized, it can be useful to apply a simple mapping function and solve only for magnetization associated with the identified units. Thus, the inverse model space is mapped onto the physical properties space to use in the forward simulation that now only depends on the specified number of properties as opposed to the number of model cells. Layers can often be identified a priori, and here we adapt the domain mapping methodology for the layer scenario. Because we deal with three different units (with a 3D magnetization), we now only solve for 3×3 parameters. Other studies have used this technique to reduce the model space from 3D to 2D or 1D, and explore physical property distribution in progressively higher dimensionality and complexity (Kang et al. 2015).

4. Results

In the following, we present the scenarios (Figure 2) using the modeling strategies described above (Figure 3). Imposed magnetizations for the different scenarios are chosen to be

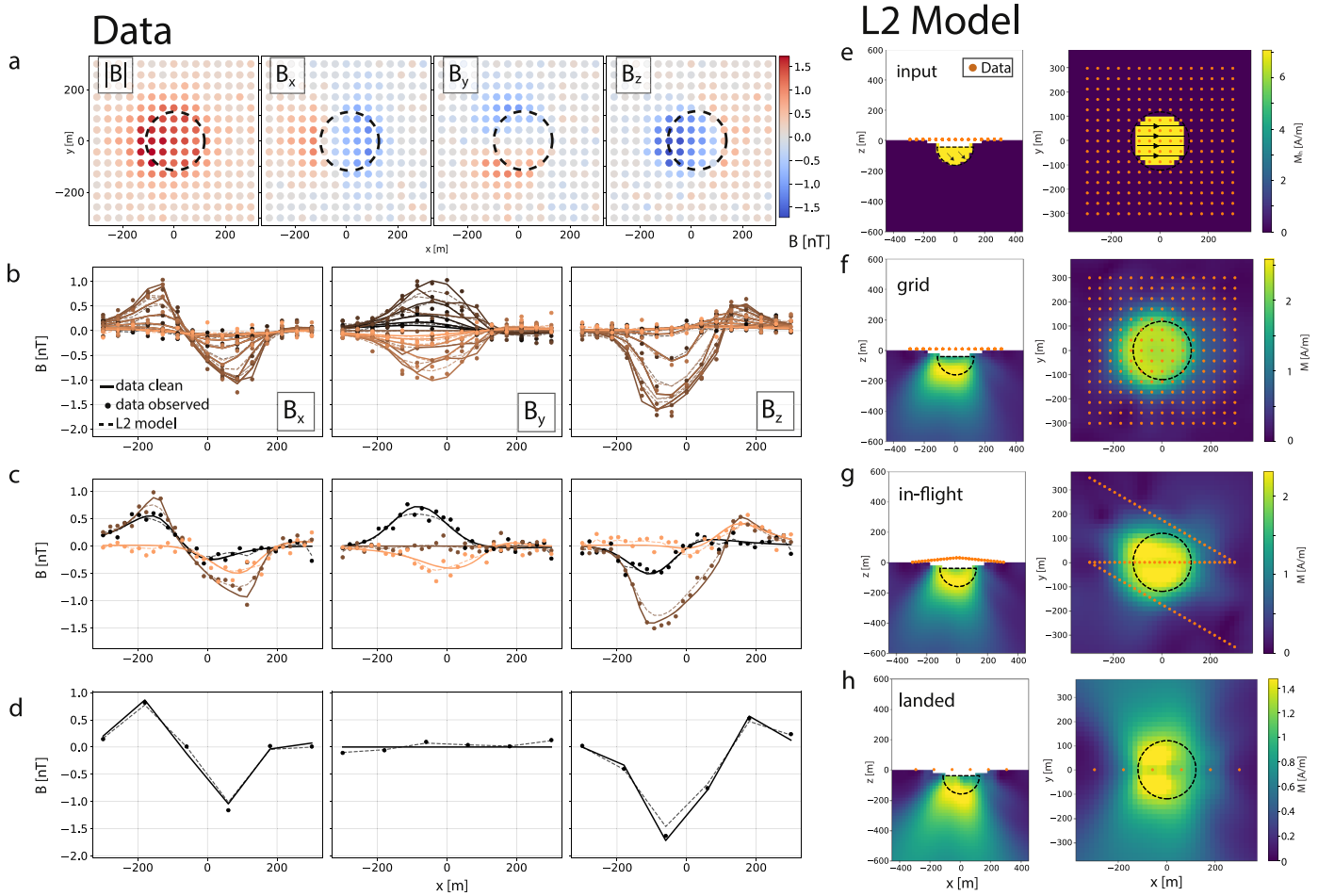

Figure 4. Scenario 1–Crater L2 inversion. (a) Different components and magnetic field amplitude of synthetic magnetic field data in the x–y plane from panel (e), a magnetization model of a crater with a total magnetization amplitude of 10 A m^{-1}, where the color bar corresponds to the magnetization amplitude in the shown plane (e.g., $M_h = \sqrt{M_x^2 + M_z^2}$ or $\sqrt{M_x^2 + M_y^2}$), and the arrows represent the third vector component (e.g., M_y or M_z). This also applies to later figures that show arrows (otherwise total amplitude is shown). (b)–(d) Different survey scenarios, (b) grid, (c) in-flight, and (d) landed, for the Bx, By, and Bz components along the track with noise added and as predicted from the L2 model. Darker to lighter colors show tracks from $-y$ to y. (f)–(h) Magnetization models of corresponding L2 inversions where the color bar represents the total magnetization amplitude, $M = \sqrt{M_x^2 + M_y^2 + M_z^2}$. The outline of the crater is marked (dashed black).

reasonable estimates based on satellite-based models and meteorites (e.g., Rochette et al. 2005; Langlais et al. 2019).

4.1. Scenario 1: Crater

The magnetized crater produces a magnetic field signature of approximately 1 nT and is seen in all components. The initial L2 inversion (Figures 4(f)–(h)) produces a relatively smeared-out picture, particularly at depth. As a result, the magnetization amplitude of the feature is underestimated, especially for the landed case, for which there are insufficient data points to determine the exact structure of the anomaly (Figure 4(h)). The model does suggest the presence of a compact feature motivating inversions using a sparse representation. The sparse model (Figures 5(a)–(c)) captures the feature extent well, especially for the dense survey coverage (Figure 5(a)). The somewhat square outline of the crater feature is the result of independent regularization of the three components in combination with poor data coverage for the in-flight and especially the landed cases (Figures 5(b) and (c)). Generally, the amplitude of the feature can be recovered well. In both the sparse and the smooth models, we observe low-amplitude magnetization in the layers closest to the surface, which is inconsistent with our model scenario (Figure 4(e)). This effect arises because of the magnetization direction (45° and downward) we have imposed on the model. As a next step, and because we have identified a compact structure consistent with the hypothesis that it is connected with the crater, we apply the parameterized approach (Figures 5(d)–(f)). We approximate the shape of the crater by a half-sphere and $\boldsymbol{m}_{\text{crater}} = [x, y, z, r, m_x, m_y, m_z] = [0, 0, -40, 120, 7, 0, -7]$. No matter the data coverage, we obtain a model representation of the magnetized crater that fits our model scenario well. Thus, even for limited data, the representation is very good and clearly better than the L2 or sparse representation.

4.2. Scenario 2: Dike

In the dike scenario, we cover a smaller area around a 15 m diameter dike due to the small horizontal extent of the feature (Figures 6(a) and (b)), and only a few data points in closest proximity to the feature are affected (Figures 6(a)–(d)). The initial L2 inversion for the dike again shows a smeared-out dike feature that, even in absence of a priori information, is localized (Figures 6(f)–(h)). Due to lacking depth sensitivity, the feature is less well resolved vertically, and we cannot probe the dike's

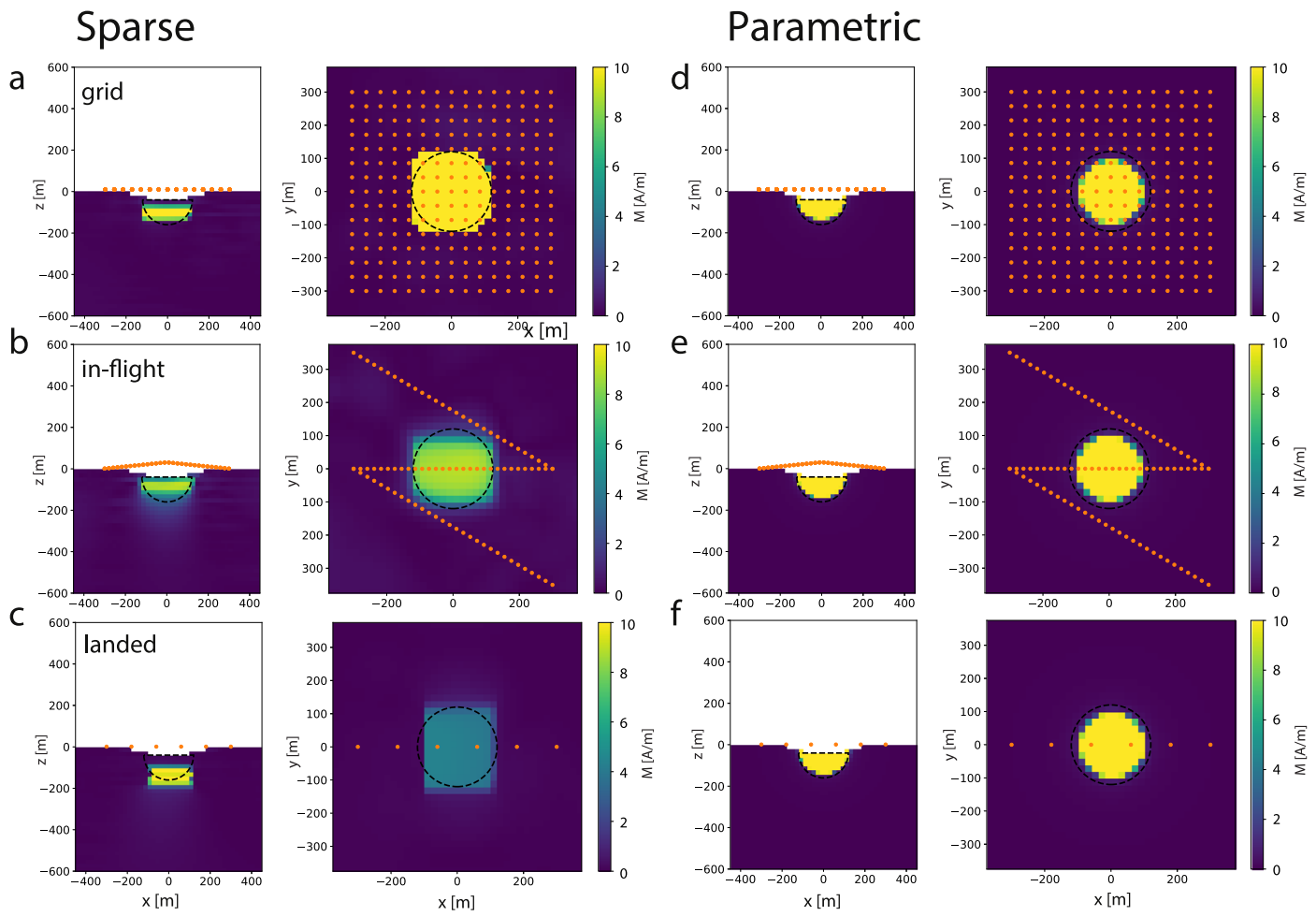

Figure 5. Scenario 1–Crater sparse and parametric inversion. Recovered models of total magnetization M for the (a)–(c) sparse and (d)–(f) parametric inversion for the different sampling geometries (a) and (d) regular grid, (b) and (e) three flight tracks, and (c) and (f) a few individual data points collected on the ground (orange). The outline of the crater is marked (dashed black). Note the change in color bar limits.

depth extent. The sparse solution enforces a compact feature and is therefore able to pinpoint the location of the dike very well, but as expected, it does not extend the feature at depth (Figures 7(a)–(c)). In places where a dike is visible via imagery and the goal is to probe whether it is (de)magnetized compared with the surrounding material, this might be sufficient. In the one-layer model, we decide to ignore depth resolution and just focus on locating the dike, which can be achieved exceptionally well (Figures 7(d)–(f)). Note that the detection of the intrusion is only possible because the data points are collected in direct proximity to the feature. For the landed case, we increased the data point density around the dike as we would in regions where such a feature is identified, e.g., in imagery. Furthermore, while we model a purely vertical and horizontally symmetric feature, we would expect some lateral extent due to smaller intrusions and heating in the surrounding crust that would increase the magnetization area and thus the area in which the feature can be detected.

4.3. Scenario 3: Layering

In the last scenario, we investigate the effect of layers that are much wider than the helicopter altitude (Figure 8(b)). Generally, a magnetic survey detects lateral gradients (Equation (1)) in magnetization. Thus, a uniformly magnetized layer of infinite extent or a uniformly magnetized shell does not lead to a magnetic field signature (Affleck 1958; Parker 1977). As a result, the traversing helicopter measures a (close to) zero magnetic field in the center of the individual layers (Figure 8(a)). Inversions without a priori information will therefore map layer edges rather than the layers themselves. This effect is clearly visible in the data (Figures 8(a)–(d)), and due to the large direction and amplitude changes across the layer boundaries, the amplitude of the magnetic field signal is larger than for previous examples, despite a similar maximum amplitude of magnetization. Note that the noise floor of 0.1 nT is low compared to the signal associated with magnetization in this example (Figures 8(b)–(d)). The edge effect is also clearly visible in the L2 inversion (Figures 8(f)–(h)), and the model predictions fit the data very well (again, as result of a comparably low noise floor). Between approximately 50 and 200 m depth, the direction of the layers can be recovered, while the inversion does not recover near surface magnetizations, as observed previously. The sparse inversion generally localizes what we see in the L2 inversion. Again, transitions can be mapped, and the magnetization direction is approximated reasonably well. Lastly, the domain mapping methodology can obtain a solution that matches the data very well (Figures 9(d)–(f)) even if only a few data are collected, as long as all units are covered. Even if no information on the direction or amplitude is provided a priori, only the layer outlines, the magnetization can

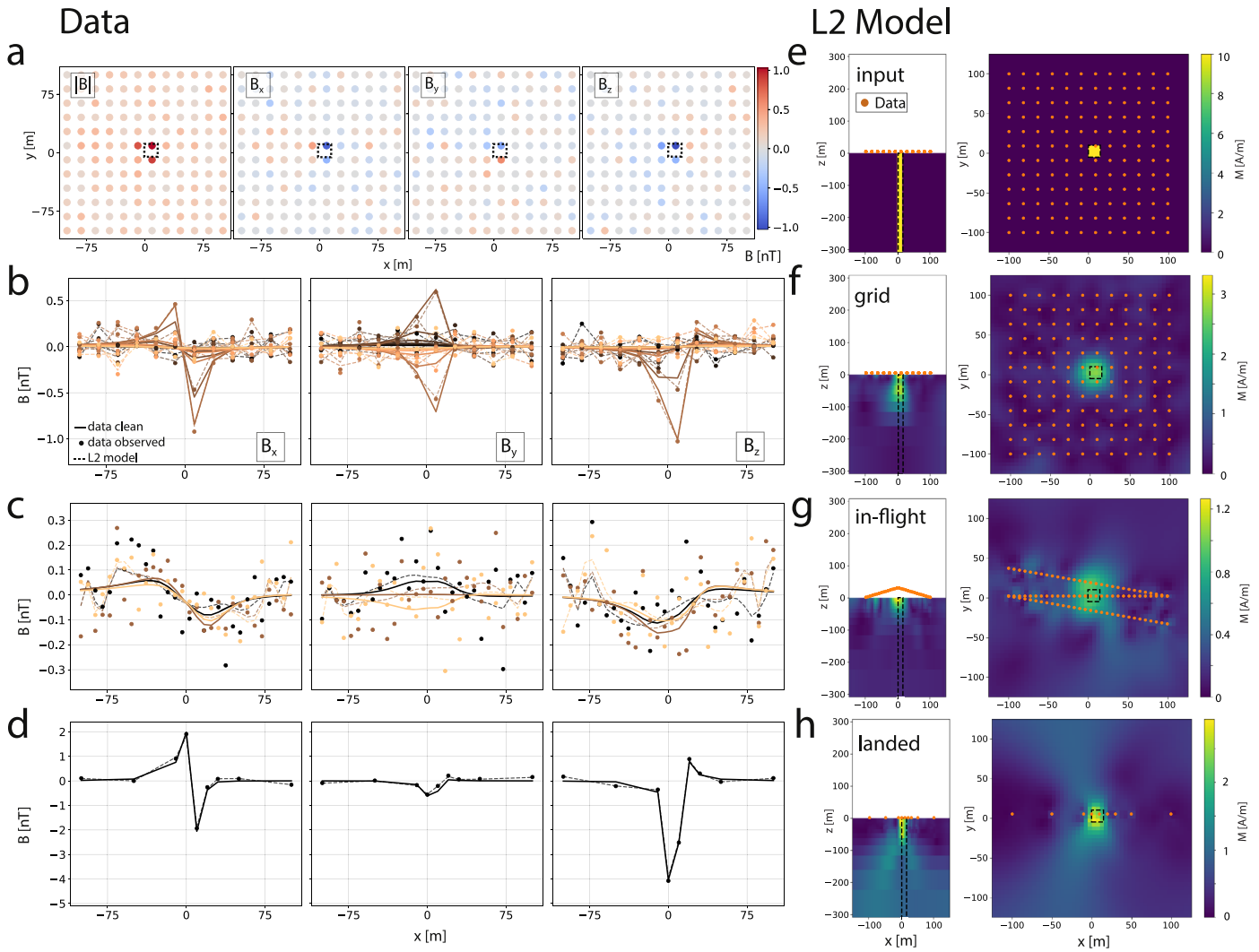

Figure 6. Scenario 2 –Dike intrusion L2 inversion. (a) Different components and magnetic field amplitudes of synthetic magnetic field data in the x–y plane from (b) a magnetization model of a crater with a total magnetization amplitude of 10 A m^{-1}. (b)–(d) Different survey scenarios, (b) mesh, (c) in-flight, and (d) landed, for the *Bx*, *By*, and *Bz* components along a track with noise added and as predicted from the L2 model as labeled. Darker to lighter colors show tracks from $-y$ to y. (f)–(h) show the magnetization models of corresponding L2 inversions. The outline of the dike intrusion is marked (dashed black).

be recovered well for all survey scenarios. This method also performs very well for high background noise (not shown) but requires good understanding of the geometry of the layers.

5. Discussion: Magnetometer Mission Considerations

5.1. Dealing with Noise

We now consider varying levels of noise. Previous figures assume a noise level of 0.1 nT, and we now investigate the effect of 0, 0.5, and 1 nT (Figure 10) for the initial L2 inversion for the crater scenario. While 0.1 nT is approximately 10% of the measured peak magnetic field, the increased noise level is substantial with respect to the crater signal. However, we can recover a coherently magnetized structure such as that shown in this example, although the magnetic field amplitude and random noise are of similar order. This is particularly encouraging, as we expect signatures associated with the surface magnetic field to mostly be stronger than what is modeled here.

Generally, noise sources are an important consideration for any magnetics mission. Above, we have described noise due to external magnetic fields; those fields will be local time–dependent and often vary on different timescales. If the duration of a helicopter traverse is much longer than the fluctuations due to the external magnetic field, we would expect the full traverse data to be affected, including crustal field anomalies. While this might lead to an under- or overestimation of the anomaly amplitude, the detection of the anomaly itself would not be impacted, except for weak magnetization sources. Periodic fluctuations on the order of minutes (i.e., comparable to a flight traverse) or seconds could affect the measurements. At InSight, these have been observed and were on the order of up to a few nanoteslas, but they only occur irregularly and usually at dusk/dawn and at night. Ionospheric fluctuations are expected, and they are strongest during the day. Hence, to mitigate external magnetic field effects, we recommend sampling at magnetically quiet times of the day or, if possible, at night. Any ROI should be covered by multiple tracks and, if possible, at similar local times. External field characterization while on the ground can be used to (i) identify the most opportune times for measurements and (ii) estimate the uncertainties associated with longer-timescale signals.

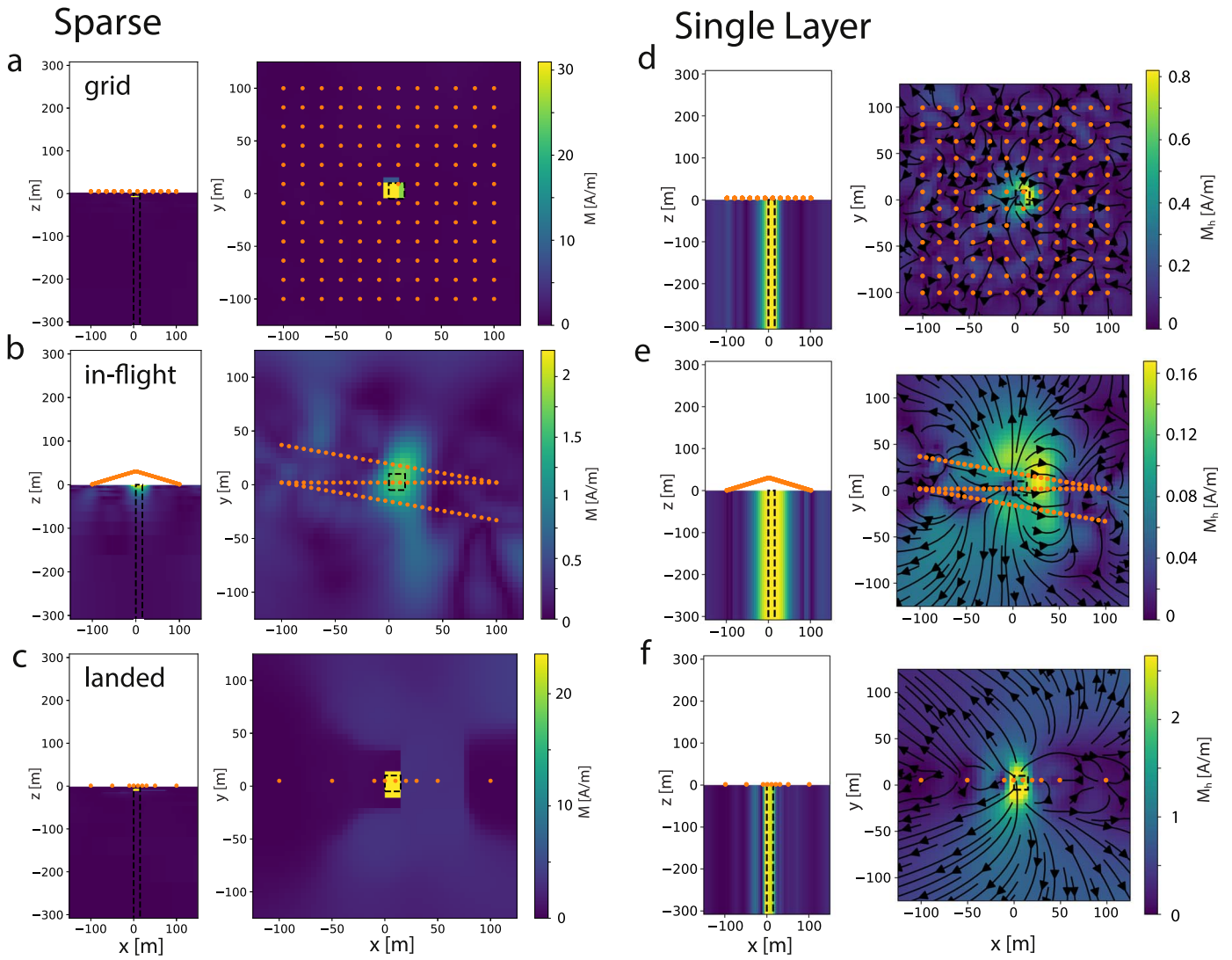

Figure 7. Scenario 2–Dike intrusion sparse and single-layer inversion. Recovered magnetization models for the (a)–(c) sparse and (d)–(f) single-layer inversion for the different sampling geometries (a) and (d) regular grid, (b) and (e) three flight tracks, and (c) and (f) a few individual data points collected on the ground (orange).

5.2. Cleanliness Considerations

Artificial sources can be substantial, and thorough cleanliness programs are essential to characterize or account for them as best as possible. Here we do not provide recommendations on cleanliness procedures but acknowledge that artificial sources might be substantial, especially for taking measurements along the flight traverse, and briefly discuss some important considerations. While low-altitude platform surveys are routinely used on Earth, we would like to note that commercial terrestrial drones are generally not designed with magnetic cleanliness in mind. Extensive characterizations of thermal effects and electric and magnetic interference are common for spacecraft missions carrying magnetometers, while terrestrial instrumentation is rarely characterized to the same degree. Spacecraft carrying science-grade magnetometers undergo magnetic cleanliness programs in order to make sure that the artificial sources are smaller than the required measurements. Such magnetic cleanliness programs are best approached from a systems-engineering perspective, working with the spacecraft, magnetometer instrument, and science teams to select best approaches (Acuña 2004).

The requirements for a mission very much depend on mission goals and landing location. Crustal magnetic fields are spatially inhomogeneous and can be very strong locally. If landing were to occur in such a location, these fields would be a dominant contribution compared with time-varying external fields and precharacterized artificial fields created by the lander/helicopter. While the latter can be large, any mission measuring ambient magnetic fields undergoes thorough investigation of artificial contributions. The requirement for accuracy of such a characterization depends on science questions. For example, accuracy to within several nanoteslas would likely be sufficient if only changes in the crustal field are of interest for a survey site in a moderately magnetized region. The noise discussion in the above subsection is relevant here.

Finally, deployable, nonmagnetic booms should be considered to move the magnetometer as far as possible from other instruments and helicopter current sources. The boom length and design will again depend on the exact measurement requirements and the nature of the artificial signals on the platform. For example, tethers have also been suggested, which would allow the magnetometer to dangle from the helicopter while traversing. In this case and ideally, inertial measurement

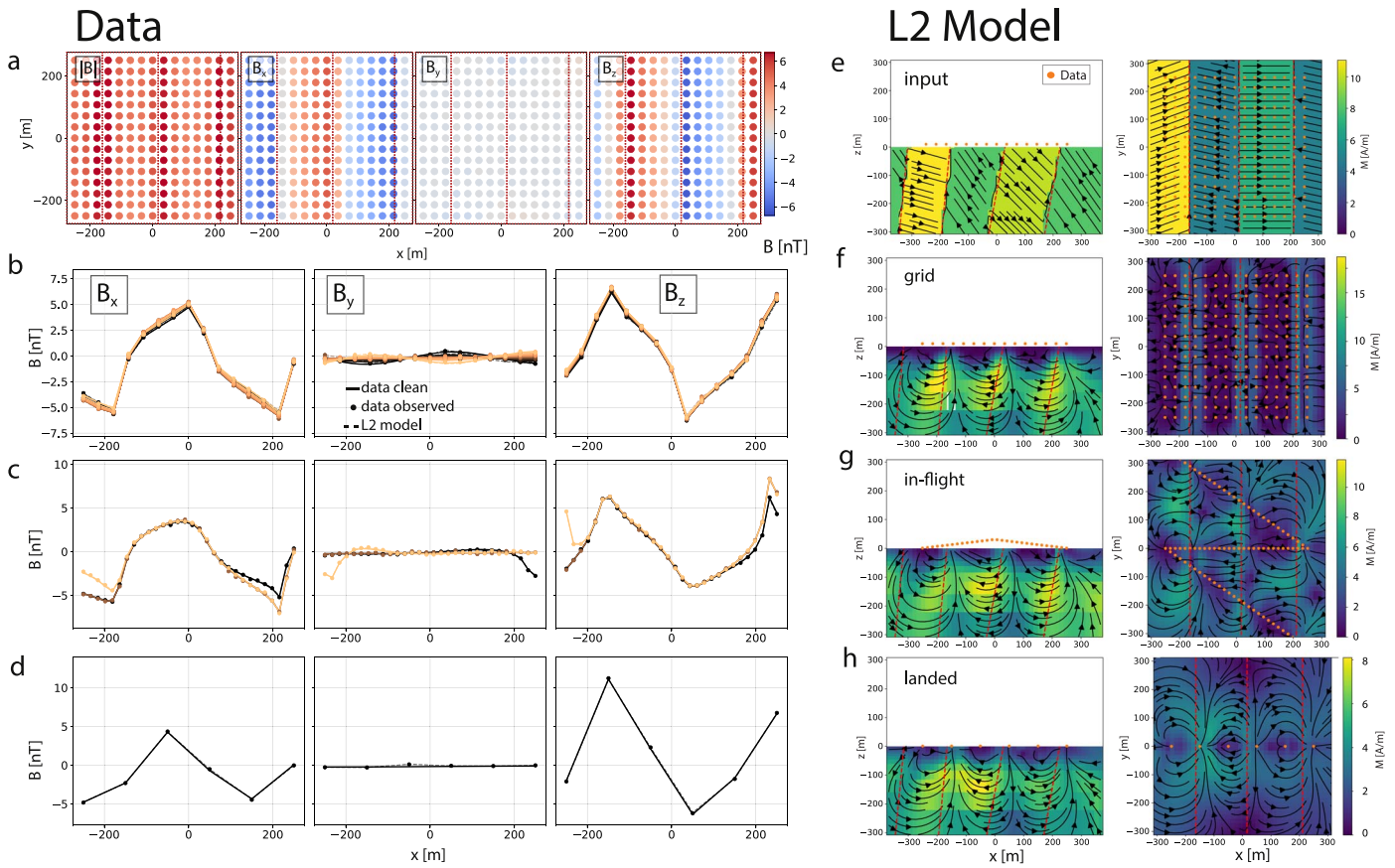

Figure 8. Scenario 3–Layers L2 inversion. (a) Different components and magnetic field amplitude of synthetic magnetic field data in the x–y plane from (b) a magnetization model of a crater with a total magnetization amplitude of 10 A m^{-1}. (b)–(d) Different sampling scenarios, (b) regular grid, (c) in-flight, and (d) landed, for the Bx, By, and Bz components along a track with noise added and as predicted from the L2 model as labeled. Darker to lighter colors show tracks from $-y$ to y. (f)–(h) show the magnetization models of corresponding L2 inversions. Layer transitions are marked (red dashed).

units could determine the instrument's position in space and allow for three component measurements; when landed, the position of the instrument could be established once and allow for reduced data collection (i.e., no constant positioning is required). The amplitude of the field would always be available and not rely on positioning. Additional lightweight magnetic sensors with varying distances to the electronics could provide further information on the fields generated by the helicopter and thus help characterize and subtract those fields (Ness et al. 1971); this, of course, would add payload mass, and this trade-off would have to be carefully considered. In all cases, the detailed design would be a collaboration between science, instrument, and spacecraft teams.

5.3. Including Other Instruments

Magnetic field data in the context of other measurements will offer the most comprehensive picture of the survey site (see also Table 1). While we do not attempt to list all possible additional instruments, we suggest a selection of data sets that could aid interpretations of magnetic field measurements.

The combination of existing orbital high-resolution imagery with an added camera on the helicopter is key for interpretation of geological surface features and their associated magnetization (e.g., Langlais & Purucker 2007; Lillis et al. 2013; Mittelholz et al. 2020a). We have shown that the inclusion of prior knowledge from imagery can greatly benefit our modeling efforts. As a further example, if we can identify a magnetic field signal associated with a pebble, rock, or block, one could use imagery to estimate its volume and thus magnetization. This would require one to move/fly around the rock at increments on the order of the size of the pebble. A similar experiment was suggested but not attempted with the robotic arm on the InSight lander (Golombek et al. 2023). Here the measurements at different distances from the pebble were planned by moving the pebble with the robotic arm. The magnetization amplitude depends on the volume extent of the magnetized structure, which can easily be misrepresented, often leading to underestimations of magnetization (see results of L2 inversions). The pebble would provide an alternative and simple way of getting at magnetization from which material properties and possibly the magnetizing field can be inferred.

Other instrumentation that would provide increased science return includes spectrometers that directly identify the elemental and/or mineralogical characteristics of surface material. This additional information can help address the carrier of magnetization and possibly magnetization acquisition mechanisms (Table 1). Landing sites with differing ROIs, e.g., highly altered versus volcanic material, would offer ideal survey sites. However, we note that spectrometers inform on surface composition, and combining these observations with the results of magnetic field inversions would require the surface layer to be magnetized. Global models for magnetization source depth mostly predict magnetization kilometers below the surface, especially in the southern hemisphere, with some regions of more surficial magnetization mostly in the

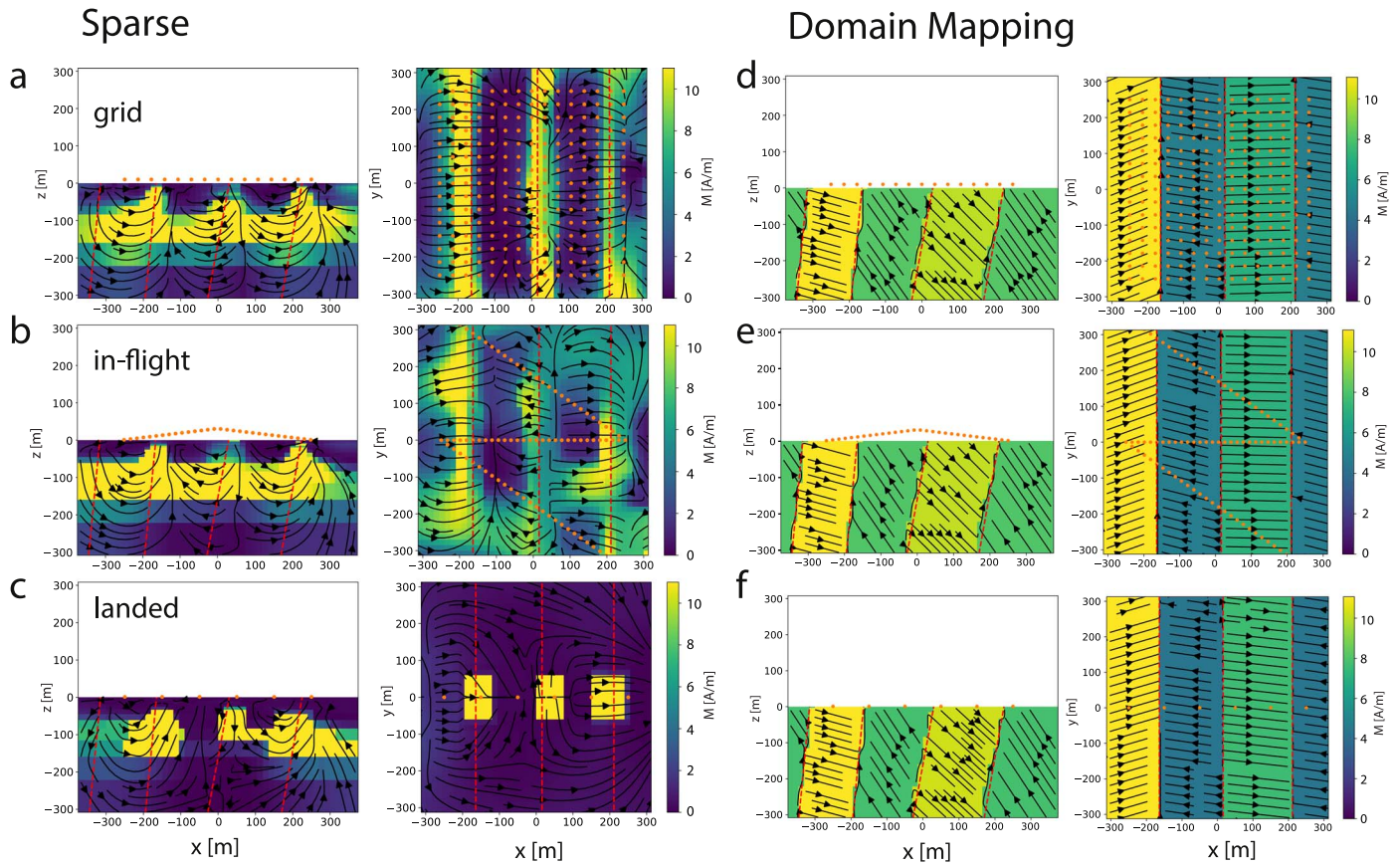

Figure 9. Scenario 3–Layers sparse and domain inversion. Recovered magnetization models for the (a)–(c) sparse and (d)–(f) domain mapping inversion for the different sampling geometries (a) and (d) regular grid, (b) and (e) three flight tracks, and (c) and (f) a few individual data points collected on the ground (orange).

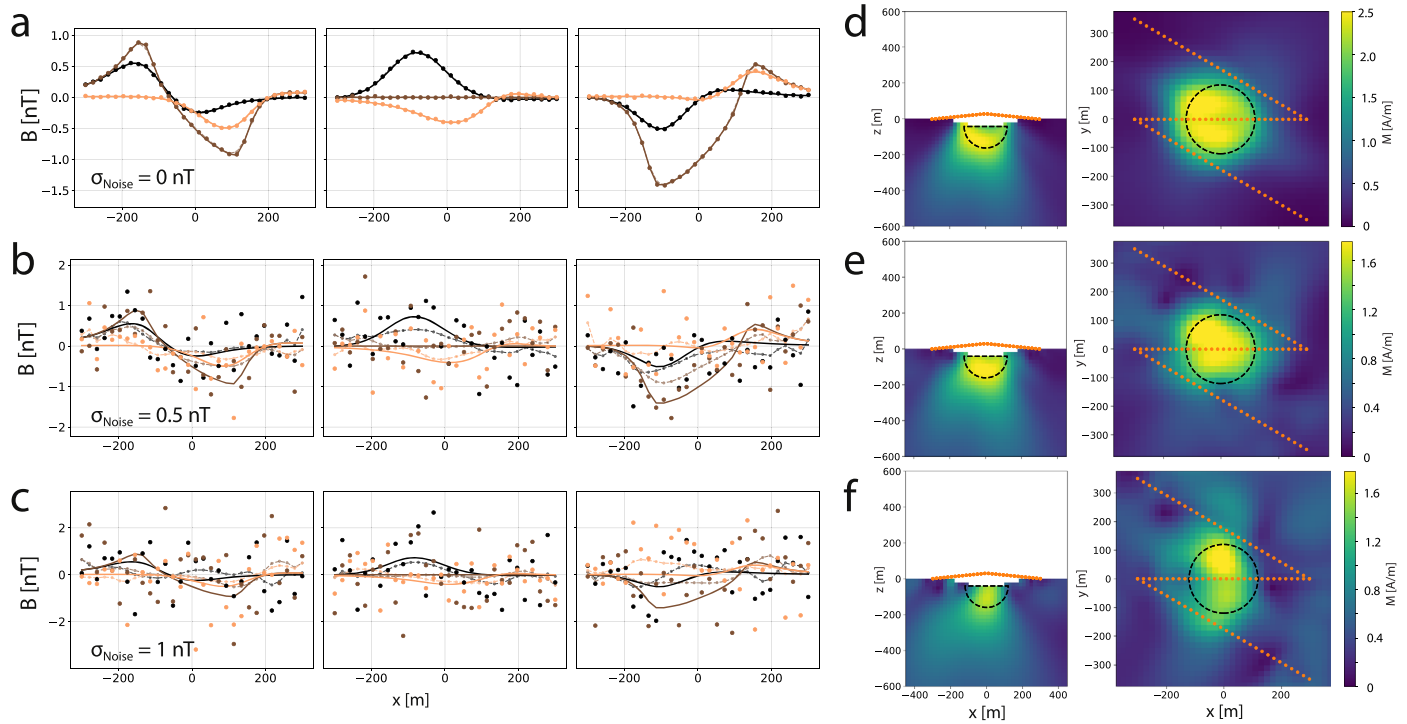

Figure 10. Scenario 1–Crater with increasing noise floor. (a)–(c) show the magnetic field signal for all three tracks due to the crater (solid line), simulated measurements including noise (dots), and the magnetic field from the recovered L2 model (dashed) at 1 m above the surface for all components. Darker to lighter colors show tracks from $-y$ to y. (d)–(f) Recovered magnetization models for the L2 inversion equivalent to Figure 4.

north (Gong & Wieczorek 2021). However, the source depth uncertainties in such models are large (Gong & Wieczorek 2021). Locally, magnetization has been shown to be at least partially surficial in the Medusa Fossae formation, particularly Lucus Planum (Mittelholz et al. 2020a; Ojha & Mittelholz 2023), and in comparison with orbital spectrometer data, composition has been shown to correlate with higher magnetic fields (AlHantoobi et al. 2021).

Lastly, information on physical properties at depth could be obtained with a gravimeter. Because gravity informs on density and thus the compositional constraints of rock, combined magnetic–gravity surveys are particularly informative in addressing the origin of magnetization. Also, because both fields fall off differently with distance to the source, they have different depth sensitivities. Joint modeling techniques for the combination of petrophysical/geological and geophysical data have been shown to more accurately represent physical properties and could provide further modeling strategies that can make use of combined data sets (e.g., Lelièvre & Farquharson 2016; Astic & Oldenburg 2019; Astic et al. 2020; Lösing et al. 2022; Moorkamp 2022).

6. Conclusion and Recommendations

We have shown that a range of methodologies will be useful to interpret magnetic field data collected by a helicopter. To summarize the lessons learned from our modeling and previous magnetic field data from Mars, we list recommendations for future helicopter surveys.

1. Landed measurements can resolve structures well, provided the measurements are made at multiple locations in proximity to the feature. However, data collected in flight will substantially increase the scientific value of the data set. Prior investigations of individual ROIs can be connected with reconnaissance flights that might uncover unexpected signals that can be used to adapt future ROIs and flight path planning.
2. Regular characterization of noise on the surface will greatly aid in separating crustal and external magnetic field signals. This could be achieved while the helicopter is charging and should cover times at which sampling is usually done.
3. Under the assumption that data can be collected in flight, flight traverses should occur at magnetically quiet times of the day or, preferably, at night, if possible. To start with, InSight observations can provide a guide to the diurnal pattern of external field fluctuations. Regular external field observations might help refine the timing for different locations.
4. Repeat measurements along horizontal traverses and vertical profiles above ROIs would enable robust identification of crustal magnetization.
5. Magnetic field observations paired with information on geology, gravity, and/or geochemistry can greatly enhance the expected science return.
6. Because magnetic fields fall off with distance from their source, robust modeling greatly benefits from several flight paths that are slightly offset and/or cover multiple altitudes.

In summary, helicopter magnetic field surveys represent a major leap forward in our understanding of the origins of Mars' crustal magnetic field and thus the evolution of terrestrial planets.

Acknowledgments

We acknowledge support from Harvard's Daly Postdoctoral Fellowship (A.M.), the Natural Sciences and Engineering Research Council of Canada (C.L.J.), and CNES in the frame of the InSight mission (B.L.). A portion of this research was carried out at the Jet Propulsion Laboratory, California Institute of Technology, under a contract with the National Aeronautics and Space Administration (80NM0018D0004). We also thank the open-source community for their ongoing contributions to SimPEG. The software is available on GitHub: https://github.com/AnnaMittelholz/Helicopter.

ORCID iDs

Anna Mittelholz https://orcid.org/0000-0002-5603-7334
Lindsey Heagy https://orcid.org/0000-0002-1551-5926
Catherine L. Johnson https://orcid.org/0000-0001-6084-0149
Jonathan Bapst https://orcid.org/0000-0003-1176-7613
Benoit Langlais https://orcid.org/0000-0001-5207-304X
Robert Lillis https://orcid.org/0000-0003-0578-517X

References

Acuña, M. H. 2004, NASA/GSFC Internal Report
Acuña, M. H., Connerney, J. E. P., Ness, N. F., et al. 1999, Sci, 284, 790
Affleck, J. 1958, Geop, 23, 738
AlHantoobi, A., Buz, J., O'Rourke, J. G., Langlais, B., & Edwards, C. S. 2021, GeoRL, 48, e0379
Antretter, M., Fuller, M., Scott, E., et al. 2003, JGRE, 108, 5049
Astic, T., Heagy, L. J., & Oldenburg, D. W. 2020, GeoJI, 224, 40
Astic, T., & Oldenburg, D. W. 2019, GeoJI, 219, 1989
Balaram, J., Aung, M., & Golombek, M. P. 2021, SSRv, 217, 56
Banerdt, W. B., Smrekar, S., Banfield, D., et al. 2020, NatGe, 13, 183
Bapst, J., Parker, T. J., Balaram, J., et al. 2021, BAAS, 53, 361
Brain, D. A., Bagenal, F., Ma, Y.-J., Nilsson, H., & Stenberg Wieser, G. 2016, JGRE, 121, 2364
Brain, D. A., Leblanc, F., Luhman, J. G., Moore, T. E., & Tian, F. 2013, in Comparative Climatology of Terrestrial Planets, Part IV: Surface and Interior, ed. M. S. J. et al. (Tucson, AZ: Univ. of Arizona), 487
Braun, R. D., Wright, H. S., Croom, M. A., Levine, J. S., & Spencer, D. A. 2006, JSpRo, 43, 1026
Brustel, C., Flahaut, J., Hauber, E., et al. 2017, JGRE, 122, 1353
Cain, J. C. 2003, JGRE, 108, 5008
Chi, P., Russell, C., Yu, Y., et al. 2019, AGUFM, 2019, DI51B–0024
Cisowski, S. M. 1986, GeCoA, 50, 1043
Cockett, R., Kang, S., Heagy, L. J., Pidlisecky, A., & Oldenburg, D. W. 2015, CG, 85, 142
Du, A., Ge, Y., Wang, H., et al. 2023, NatAs, in press
Dunlop, D. J., & Arkani-Hamed, J. 2005, JGRE, 110, E12S04
Emoto, K., Takao, Y., & Kuninaka, H. 2018, Biological Sciences in Space, 32, 1
Fournier, D., Heagy, L. J., & Oldenburg, D. W. 2020, Geop, 85, J33
Fournier, D., & Oldenburg, D. W. 2019, GeoJI, 218, 268
Gattacceca, J., Berthe, L., Boustie, M., et al. 2008, PEPI, 166, 1
Gattacceca, J., Hewins, R. H., Lorand, J.-P., et al. 2013, M&PS, 48, 1919
Golombek, M., Hudson, T., Bailey, P., et al. 2023, SSRv, 219, 20
Gong, S., & Wieczorek, M. 2021, JGRE, 126, e06690
Hall, J. L., Pauken, M. T., Kerzhanovich, V. V., et al. 2007, in AIAA Balloon Systems Conf. (Reston, VA: AIAA), 1
Herring, T., Heagy, L. J., Pidlisecky, A., & Cey, E. 2022, CG, 159, 104986
Jakosky, B. M., Lin, R. P., Grebowsky, J. M., et al. 2015, SSRv, 195, 3
Johnson, C. L., Mittelholz, A., Langlais, B., et al. 2020, NatGe, 13, 199
Johnson, C. L., & Phillips, R. J. 2005, E&PSL, 230, 241
Kang, S., Cockett, R., Heagy, L. J., & Oldenburg, D. W. 2015, SEG Technical Program Expanded Abstracts, 2015, 5000
Kirschvink, J. L., Maine, A. T., & Vali, H. 1997, Sci, 275, 1629
Knapmeyer-Endrun, B., Panning, M. P., Bissig, F., et al. 2021, Sci, 373, 438

Langlais, B., Civet, F., & Thébault, E. 2017, JGRE, 122, 110
Langlais, B., & Purucker, M. 2007, P&SS, 55, 270
Langlais, B., Thébault, E., Houliez, A., Purucker, M. E., & Lillis, R. J. 2019, JGRE, 124, 1542
Le Deit, L., Bourgeois, O., Mège, D., et al. 2010, Icar, 208, 684
Lelièvre, P. G., & Farquharson, C. G. 2016, in Integrated Imaging for Mineral Exploration, ed. M. Moorkamp et al. (Washington, DC: AGU), 137
Lelièvre, P. G., & Oldenburg, D. W. 2009, Geop, 74, L21
Lillis, R. J., Fillingim, M. O., Ma, Y., et al. 2019, GeoRL, 46, 5083
Lillis, R. J., Manga, M., Mitchell, D. L., Lin, R. P., & Acuña, M. H. 2006, GeoRL, 33, L03202
Lillis, R. J., Robbins, S., Manga, M., Halekas, J. S., & Frey, H. V. 2013, JGRE, 118, 1488
Liu, K., Hao, X., Li, Y., et al. 2020, E&PP, 4, 384
Lösing, M., Moorkamp, M., & Ebbing, J. 2022, GeoJI, 232, 162
Luo, H., Du, A. M., Ge, Y. S., et al. 2022, JGRE, 127, e07112
Mayhew, M. 1979, JGZG, 45, 119
Mier-Hicks, F., Grip, H. F., Kalantari, A., et al. 2023, in 2023 IEEE Aerospace Conf. (Piscataway, NJ: IEEE), 1
Mitteholz, A., & Johnson, C. L. 2022, FrASS, 9, 895362
Mittelholz, A., Espley, J., Connerney, J., et al. 2021a, BAAS, 53, 006
Mittelholz, A., Johnson, C. L., Feinberg, J. M., Langlais, B., & Phillips, R. J. 2020a, SciA, 6, eaba0513
Mittelholz, A., Johnson, C. L., Fillingim, M., et al. 2021b, GeoRL, 48, e95432
Mittelholz, A., Johnson, C. L., Fillingim, M., et al. 2023, JGRE, 128, e2022JE007616
Mittelholz, A., Johnson, C. L., & Morschhauser, A. 2018, GeoRL, 45, 5899
Mittelholz, A., Johnson, C. L., Thorne, S. N., et al. 2020b, JGRE, 125, 1
Mohit, P. S., & Arkani-Hamed, J. 2004, Icar, 168, 305
Moore, K. M., & Bloxham, J. 2017, JGRE, 122, 1443
Moorkamp, M. 2022, GeoRL, 49, e96336
Morschhauser, A., Lesur, V., & Grott, M. 2014, JGRE, 119, 1162
Nedell, S. S., Squyres, S. W., & Andersen, D. W. 1987, Icar, 70, 409
Ness, N. F., Behannon, K. W., Lepping, R. P., & Schatten, K. H. 1971, JGR, 76, 3564
Nimmo, F., & Stevenson, D. J. 2000, JGR, 105, 11969
Ojha, L., & Mittelholz, A. 2023, Icar, 395, 115471
Parker, R. L. 1977, AREPS, 5, 35
Pieterek, B., Ciazela, J., Lagain, A., & Ciazela, M. 2022, Icar, 386, 115151
Purucker, M., Ravat, D., Frey, H., et al. 2000, GeoRL, 27, 2449
Ramstad, R., & Barabash, S. 2021, SSRv, 217, 36
Rapin, W., Fraeman, A., Ehlmann, B., et al. 2021, BAAS, 53, 221
Ravat, D. 2011, Icar, 214, 400
Robbins, S. J., Hynek, B. M., Lillis, R. J., & Bottke, W. F. 2013, Icar, 225, 173
Rochette, P., Gattacceca, J., Chevrier, V., et al. 2005, M&PS, 40, 529
Shaw, J., Hill, M. J., & Openshaw, S. J. 2001, E&PSL, 190, 103
Smrekar, S. E., Lognonné, P., Spohn, T., et al. 2018, SSRv, 215, 3
Stähler, S. C., Mittelholz, A., Perrin, C., et al. 2022, NatAs, 6, 1376
Steele, S. C., Fu, R. R., Volk, M. W., et al. 2023, SciA, 9, eade9071
Tanaka, K. L., Skinner, J. a., Dohm, J. M., et al. 2014, Geologic Map of Mars Scientific Investigations Map 3292, USGS
Thomas, P., Grott, M., Morschhauser, A., & Vervelidou, F. 2018, JGRE, 123, 1140
Thorne, S. N., Johnson, C. L., Mittelholz, A., et al. 2022, P&SS, 217, 105487
Tikhonov, A. N., Goncharsky, A. V., Stepanov, V. V., & Yagola, A. G. 1995, Numerical Methods for the Solution of Ill-posed Problems, Vol. 328 (Dordrecht: Springer)
Tikoo, S. M., & Evans, A. J. 2022, AREPS, 50, 99
Vervelidou, F., Lesur, V., Grott, M., Morschhauser, A., & Lillis, R. J. 2017, JGRE, 122, 2294
Vine, F. J., & Matthews, D. H. 1963, Natur, 199, 947
Volk, M. W., Fu, R. R., Mittelholz, A., & Day, J. M. 2021, JGRE, 126, e06856
Wieczorek, M. A., Broquet, A., McLennan, S. M., et al. 2022, JGRE, 127, e07298
Yingst, R. A., Johnson, J. R., Banfield, D., et al. 2022, MEPAG, https://mepag.jpl.nasa.gov/about.cfm